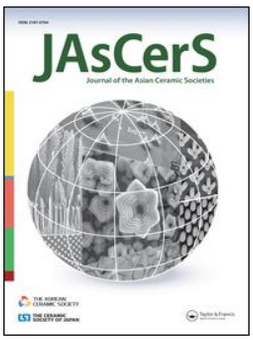

Journal of Asian Ceramic Societies

ISSN: (Print) (Online) Journal homepage: https://www.tandfonline.com/loi/tace20

Effect of doping (with cobalt or nickel) and UV exposure on the antibacterial, anticancer, and ROS generation activities of zinc oxide nanoparticles

Prashanth G K , P. A. Prashanth , Padam Singh , B. M. Nagabhushana , C. Shivakumara , Krishnaiah G M , H. G. Nagendra , H. M. Sathyananda & Vinita Chaturvedi

To cite this article: Prashanth G K , P. A. Prashanth , Padam Singh , B. M. Nagabhushana , C. Shivakumara , Krishnaiah G M , H. G. Nagendra , H. M. Sathyananda & Vinita Chaturvedi (2020): Effect of doping (with cobalt or nickel) and UV exposure on the antibacterial, anticancer, and ROS generation activities of zinc oxide nanoparticles, Journal of Asian Ceramic Societies, DOI: 10.1080/21870764.2020.1824328

To link to this article: https://doi.org/10.1080/21870764.2020.1824328

Published online: 29 Sep 2020.

JOURNAL OF ASIAN CERAMIC SOCIETIES
https://doi.org/10.1080/21870764.2020.1824328

Effect of doping (with cobalt or nickel) and UV exposure on the antibacterial, anticancer, and ROS generation activities of zinc oxide nanoparticles

Prashanth G K[a,b], P. A. Prashanth[b,c], Padam Singh[d,e], B. M. Nagabhushana[f], C. Shivakumara[g], Krishnaiah G M[a], H. G. Nagendra[h], H. M. Sathyananda[a] and Vinita Chaturvedi[e]

[a]Department of Chemistry, Sir M. Visvesvaraya Institute of Technology, Bengaluru, India, Affiliated to Visvesvaraya Technological University, Belagavi, India; [b]Centre for Research and Evaluation, Bharathiar University, Coimbatore, India; [c]Department of Chemistry, PES College of Engineering, Mandya, India, Affiliated to Visvesvaraya Technological University, Belagavi, India; [d]Vaccine and Infectious Disease Research Centre, Translational Health Science and Technology Institute, Faridabad, India; [e]Biochemistry Division, Central Drug Research Institute, CSIR, Lucknow, India; [f]Visvesvaraya Technological University, Belagavi, India, Bengaluru, India; [g]Solid State and Structural Chemistry Unit, Indian Institute of Science, Bengaluru, India; [h]Department of Bio Technology, Sir M. Visvesvaraya Institute of Technology, Bengaluru, India, Affiliated to Visvesvaraya Technological University, Belagavi, India

ABSTRACT

We describe the synthesis, structural and morphological characteristics of cobalt and nickel doped zinc oxide nanoparticles (ZnO NPs) by solution combustion technique by utilizing lemon juice as bio-fuel. Structural parameters were confirmed by the X-ray Rietveld refinement method, all the compounds were crystallized in the wurtzite hexagonal structure with space group *P63mc* (No. 186). Field emission scanning electron microscopy coupled with energy dispersive X-ray elemental mapping results revealed agglomerated spherical shaped particles and dopant ions were homogeneously distributed. Antibacterial, anticancer, and reactive oxygen species (ROS) generation activities were studied on undoped ZnO-, Co-, and Ni-doped ZnO nanoparticles upon un-exposed/exposed to ultraviolet radiations at 300 nm for 1 h. Antibacterial studies were performed against *Salmonella enterica* and *Clostridium perfringens*. Anticancer activity was tested on HeLa and MCF-7 cell lines. Generation of ROS was studied in J744 mouse macrophage cells. Doping of cobalt or nickel in the ZnO lattice enhanced antibacterial, anticancer, and oxidative response generation activities compared to undoped ZnO NPs. These activities were further improved upon exposure to ultraviolet radiations. Together, data indicate a direct activity of ZnO NPs against bacteria, cancer cells and simultaneously boosting host's immunity via inducing activation of immune cells (mouse macrophage cells).

ARTICLE HISTORY
Received 31 May 2020
Accepted 10 September 2020

KEYWORDS
Co/Ni doped ZnO; UV exposure; ROS measurement; flow cytometer; antimicrobial; cytotoxicity

1. Introduction

The use of ZnO nanoparticles (NPs) for anticancer and antibacterial treatments has been previously well demonstrated by many researchers. ZnO NPs have received considerable attention in recent days for their use as anti-virals [1–3]. Various shapes and sizes were tried and some form of difference was found. However, ZnO being a semiconductor material, we wanted to understand how we could use this property to our advantage. It was found from the literature which showed that ZnO tetrapods were better able to adsorb buffer onto their surface when they were exposed to UV rather than when unexposed [4]. We wanted to understand how we could further increase the efficacy of these particles. Literature survey indicated that the best way to enhance these properties was by doping the particles with other transition metal ions which could enhance the UV absorption property.

Hence, in the present work, Cobalt (Co) and Nickel (Ni) have been chosen as model transition metal ions to dope into ZnO. There are only few reports on the antimicrobial and anticancer activities of Co and Ni-doped ZnO NPs. Recently, many complexes and nanomaterials of Co (II) showing antimicrobial activity have been reported [5]. Most of those studies were primarily focused on optical, electrical, and magnetic properties of Co-doped ZnO NPs [6]. Also few attempts to consider the antimicrobial properties of Co-doped ZnO NPs have been made in the past. Co-doped ZnO NPs show higher activity as an antimicrobial agent against *Salmonella typhi, Staphylococcus aureus, Bacillus cereus, Escherichia coli, Pseudomonas aeruginosa (P. aeruginosa)*, and *Candida albicans (C. albicans)* compared to undoped ZnO NPs [7]. Ni-doped ZnO NPs demonstrated stronger antibacterial activity against *P. aeruginosa* and *Bacillus subtilis* than the undoped ZnO NPs [8]. Cytotoxcity of Ni-doped ZnO NPs against HEK293T and HEp2 cell lines has also been reported [9]. Experimental results have also indicated that the assimilation of Ni into the ZnO matrix has a beneficial effect on the antimicrobial activity of ZnO NPs, and enhances the ability of the ZnO NPs to kill the fungi *C. albicans* [9].

Solution combustion synthesis (SCS) is an exciting technique, which involves propagation of self-

CONTACT Prashanth G.K prashaanthgk@gmail.com; prashanth_chem@sirmvit.edu Assistant Professor, Department of Chemistry, Sir M. Visvesvaraya Institute of Technology, Bengaluru-562157

sustained exothermic reactions along with an aqueous or sol–gel media. SCS has been utilized to synthesize a number of NPs such as ZnO, CuO, MgO, Al_2O_3, $MgAl_2O_4$ using numerous organic compounds such as urea, oxalyl dihydrazide, citric acid, glycine as fuels [10–13]. SCS has many advantages over other methods and using plant extracts as reducing agents compared to chemicals being used as reductants [14]. Green synthesis approach for the synthesis of metal NPs has many different advantages over different strategies like it's extremely straightforward, clean, efficient, economically low cost as bio-resources are used which will act as reducer furthermore as stabilizing agent and capping agent. It is a nontoxic technique because of less or nonconsumption of unsafe materials on the surface of nanomaterials, it doesn't want any external ligand or capping or stabilizing agent for NPs [15–21]. Additionally to any or all these biosynthesized NPs are usually biocompatible and extremely applicable for medical specialty applications [15–17]. Green syntheses of different NPs by plants extracts such as rose [22], lucerne [23], pomegranate, tamarind [24], *Ceraus japonica* [25], cannon ball [26], borage [27], lemon juice [28], rosemary [29], *Ailanthus* [30], *Aloe vera* [31], *Rieshi mushroom* [32] etc., have been reported. In our earlier studies, we have reported the advantages of using lemon juice as a reductant over its chemical counterpart citric acid in SCS [33]. Hence, lemon juice has been employed as bio fuel to dope ZnO by SCS. Co and Ni metal ions at different concentrations (1 to 9 mol percent) were doped into ZnO by SCS using lemon juice as bio-fuel. All the samples were subjected to extensive characterization by powder X-ray diffraction (PXRD), field emission scanning electron microscopy (FESEM) with energy dispersive spectroscopy (EDS), and inductively coupled plasma optical emission spectrometry (ICP-OES). The samples were tested for their antibacterial activity against *Salmonella enterica (S. enterica)* and *(C. perfringens)*. Anticancer activity of the samples was tested on HeLa and MCF-7 cancer cell lines and normal 3T3-L1 cells, by 3-[4, 5-dimethylthiazol-2-yl]-2,5-diphenyl tetrazolium bromide (MTT) assay. Fluorescence-activated cell sorting (FACS) using 2′,7′-dichlorodihydrofluorescein diacetate (H_2DCFDA) was used to assess the generation of ROS in J774 mouse macrophage cells.

2. Materials and methods

2.1. Materials

Zinc nitrate hexahydrate [$Zn(NO_3)_2.6H_2O$, AR, 99% SD Fine], Dulbecco's Modified Eagle's medium [DMEM, Gibco], Dimethyl sulfoxide [DMSO, C_2H_6SO, AR, 99% Merck], 3-[4, 5-dimethylthiazol-2-yl]-2,5-diphenyl tetrazolium bromide [MTT, $C_{18}H_{16}BrN_5S$, 97.5%, Sigma Aldrich], Cobaltous nitrate hexahydrate [$Co(NO_3)_2.6H_2O$, Fisher, AR grade], Nickel nitrate hexahydrate [$N_2NiO_6.6H_2O$, Kemphasol, AR grade], ZnO NPs [Commercial, < 100 nm, Sigma], Tryptic soya broth [Sigma Aldrich], 2′,7′-dichlorodihydrofluorescein diacetate [H_2DCFDA, Sigma Aldrich], Mueller Hinton broth [MH broth, Himedia] were procured commercially and fresh lemons were purchased from the local market.

2.2. Synthesis of undoped, Co- and Ni-doped ZnO NPs by SCS

Synthesis of undoped, Co- and Ni-doped NPs using lemon juice as bio-fuel has been carried out as described in our earlier report [28]. In short, filtered fresh lemon juice (4.5 mL) and $Zn(NO_3)_2.6H_2O$ (2.0 g) were taken in 20 mL of double distilled H_2O and dissolved fully beneath stirring. The mixture-containing crystallizing dish was put in an extremely preheated muffle furnace held at 375 ± 10°C. Within a brief time the solution stewed to create a transparent gel followed by the fuel being easily combusted.

Nanocrystalline samples of $Zn_{1-x}Co_xO$ and $Zn_{1-x}Ni_xO$ (x = 0.01, 0.03 0.05, 0.07 and 0.09) were synthesized. All the samples were subjected to calcination at 600°C for 3 h.

2.3. Characterization techniques

Powder X-ray diffraction (PXRD) patterns for all the samples were recorded on a Panalytical X'Pert Pro MPD powder diffractometer using Ni-filtered Cu Kα radiation (λ = 1.5418 Å) as the source. For Rietveld refinement, the data were collected at a scan rate of 2°/min with a 0.02° step size for 2θ from 10° to 80°. Rietveld refinement method was employed to refine the structural parameters using FullProf Suite-2000 program. Surface morphology of the samples was studied by FE-SEM performed on Nova Nano SEM-450. The EDS investigated the compositional properties of the ZnO, Co- and Ni-doped ZnO NPs. ICP-OES measurements were carried out on Perkin Elmer Optima 5300 to quantify the elemental concentration with the sample.

2.4. Evaluation of antibacterial activity

For the evaluation of antibacterial activity two bacteria, namely *Salmonella enterica* (*S. enterica)* and *Clostridium perfringens* (*C. perfringens*) were included in the study. Bacterial cultures *S. enterica* ATCC 14028 and *C. perfringens* ATCC 13124 were procured from American type

culture collection (ATCC). These two bacteria are important from the view point of human health. *S. enterica* is a Gram negative bacterium, a subsp of it *S. typhi* causes typhoid fever. Infection begins with the activity of contaminated food or water so salmonellae reach the internal organ epithelial tissue and trigger gastrointestinal illness. The other one *C. perfringens* is a Gram positive bacterium causes food poisoning. This commonly occurs when cooked food that is infected with the bacteria is left out, which allows rapid multiplication of *C. perfringens*. The illness is the consequence of intestinal toxin development. *C. perfringens* is also known to cause other illness including infections of the skin and deeper tissues. The emergence of infectious diseases poses a significant threat to public health, particularly with the emergence of antibiotic-resistant microorganism strains. Generally, each gram positive and gram negative microorganism is thought to present a significant public pathological state.

Cell suspensions from bacterial cultures grown on tryptic soya broth (adjusted to 1–2 × 10^5 cells/mL) were used as inocula. Homogeneous aqueous dispersions of ZnO NPs of 1.953–1000 µg/mL (two-fold dilutions) in MH broth were assessed against the cultures. 75 µL of the dispersion of NPs of different concentrations was mixed with 10 mL bacterial inoculum in 96-well plates in triplicate. 75 µL of RPMI media (MH agar) without NPs mixed with 10 mL inocula was used as the control. Treated bacterial cultures were incubated at 35°C. The test plates were observed after 18–20 h and optical density was measured at 600 nm in tecan plate reader.

% inhibition was calculated as follows:

$$\frac{[Absorbance\,of\,control(untreated) - Absorbance(treated)]}{Absorbance\,of\,control} \quad (1)$$

Minimum inhibitory concentration (MIC) was calculated as the minimum concentration of NPs with an OD inhibition of at least 50% compared to the control.

The same procedure was repeated by exposing the NPs for 1 h to UV light at 300 nm (Philips TUV 30 W G30T8) and then the measurements were carried out.

2.5. Evaluation of anti-carcinogenic activity and cytotoxicity

Anti-carcinogenic response of ZnO NPs was evaluated by MTT assay as explained in our previous reports on cervical cancer cell line HeLa and breast cancer cell line MCF-7 with slight modifications [28,33–37]. These cells (procured from ATCC) of 80% confluent were trypsinized.

The viable cells were plated in 96-well plates at a density of 2 × 10^5 cells/well. Cells were exposed to 0–320 µg/mL of undoped, cobalt,- and nickel-doped ZnO NPs for 24 h. Following this, MTT was added in the wells, and plates were incubated for 3–4 h further. The reaction mixture was taken out and 100 µL/well DMSO was added and mixed several times by pipetting up and down. The absorbance of plates was recorded at 590 nm. Outcomes were expressed as percentage of control. The percentage growth inhibition was calculated using the following formula and concentration of NPs needed to inhibit the cell growth by 50% (IC50) values were generated from the dose-response curves for each cell line.

$$\%\ of\ inhibition = \begin{bmatrix} (OD\ of\ Control - OD\ of\ sample)/ \\ OD\ of\ Control * 100 \end{bmatrix} \quad (2)$$

Following the same technique, the cytotoxicity of the samples was also assessed against normal 3T3-L1 (fibroblast-like cells derived from mouse embryos).

The dispersions of NPs were exposed to UV light (300 nm) for 1 h and the same procedure was repeated.

2.6. Determination of ROS generation

ROS generation is inevitable for aerobic species, and occurs at a regulated pace in healthy cells. ROS production is significantly increased under conditions of oxidative stress, resulting in subsequent alterations of membrane lipids, proteins, and nucleic acids. Oxidative damage to these bio-molecules is associated with aging as well as a number of adverse events including atherosclerosis, carcinogenesis, exposure to ischemic reperfusion, and neurodegenerative disorder.

Estimation of ROS generation was carried out using H_2DCFDA [38]. The cell-permeable H_2DCFDA is a chemically reduced form of fluorescein used as an indicator for reactive oxygen species (ROS) in cells (neutrophils and macrophages) by detecting the generation of reactive oxygen intermediates. Upon cleavage of the acetate groups by intracellular esterases and oxidation, the non-fluorescent H_2DCFDA is converted to a highly fluorescent 2′,7′-dichlorofluorescein (DCF) with absorption/emission maximum at ~492–495/517–527 nm. Fluorescence can be monitored using a flow cytometer, fluorometer, microplate reader, or fluorescence microscope, using excitation sources and filters appropriate for fluorescein. Here, the measurements of UV-unexposed and UV-exposed samples were carried out in J774 Mouse macrophage cell line (derived from a murine reticulum cell sarcoma).

Samples used were, undoped ZnO NPs, ZnO- NPs-doped separately with, 9 and 1 mol percent of Co and Ni and ZnO procured from Sigma (USA) as a reference. Two-fold concentrations, from 50.0 to 0.39 µg/mL of all the test samples were prepared in DMEM and divided into two sets. One set of the samples was

exposed to UV radiations (300 nm) for 1 h. H_2O_2 0.01% was used as positive control. Wells containing dye (H_2DCFDA) only, served as negative control.

ROS production was measured in Real Time format by recording the Relative Fluorescence Units (RFUs) up to 80 min time period at the interval of 10 min each. Actual values were calculated by making auto correction by subtracting the fluorescence appeared in the wells having cells and dye only (Blanks). 0.01% H_2O_2 was used as a positive control. Effect of UV exposure on ROS generation by mouse macrophage cells was observed by calculating the differences in RFUs by subtracting the values of UV-unexposed samples from the UV-exposed ones.

3. Results and discussion

3.1. X-ray diffraction analysis

The Powder X-ray diffraction patterns of undoped ZnO, cobalt, and nickel-doped ZnO NPs are shown in Figure 1. The intense peaks revealed the crystalline nature of the samples. From Figure 1(a) in undoped ZnO compound, all the diffraction peaks correspond to a hexagonal wurtzite structure having the space group *P63mc* (no. 186), which is in agreement to the standard Joint Committee on Powder Diffraction Standards

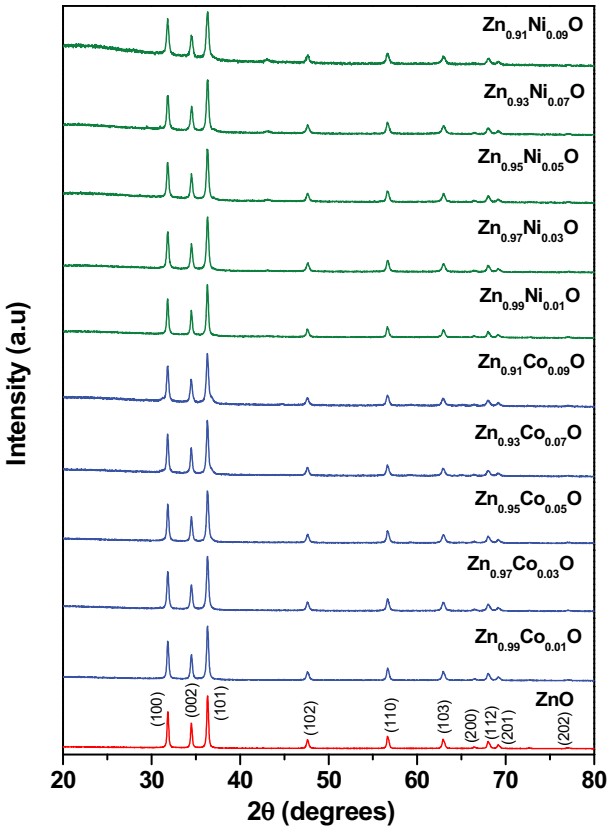

Figure 1. Powder X-ray diffraction patterns of ZnO, Co and Ni doped ZnO NPs.

(JCPDS) card No. 80–0075. Further, trivalent cobalt and divalent nickel ions were substituted to divalent zinc site in the ZnO lattice. In case of cobalt-substituted compounds, Co^{3+} and Zn^{2+} – ions are having almost same ionic radii ($r_{Co}{}^{3+}$ = 0.61 Å and $r_{Zn}{}^{2+}$ = 0.60 Å). On substitution of 6-coordinated Co^{3+} ion ($r_{Co}{}^{3+}$ = 0.61 Å) to Zn^{2+} ion ($r_{Zn}{}^{2+}$ = 0.60 Å), up to 5 mol % we did not see any impurity lines of Co_3O_4 in the powder XRD patterns. Whereas, 7 and 9 mol % of cobalt-substituted compounds exhibited small shoulder/peak around 2 theta 37 and 45 in the powder XRD patterns. Whereas nickel doped compounds, 4-coordinated Ni^{2+} – ion having smaller ionic radii ($r_{Ni}{}^{2+}$ = 0.55 Å) than 4-coordinated Zn^{2+} ion ($r_{Zn}{}^{2+}$ = 0.60 Å), we do observe small impurity lines of NiO around 2 theta 37 and 43 of 3 mol % nickel doped compound. On increasing nickel content, these peaks gradually increased. This indicates that, certain amount of Co^{3+} or Ni^{2+} – ions are substituting to Zn^{2+} – site in the ZnO lattice. We do observe around 2% impurity lines of Co_3O_4 and NiO in the 9 mol % cobalt and nickel doped compounds.

The structural parameters for all the compounds were refined from the Rietveld method using powder XRD data. The refinement results confirmed that all the samples were crystallized in the hexagonal wurtzite structure with space group *P63mc* (no. 186) and the refined lattice parameters and unit cell volumes are summarized in Table 1. It was noted that there were no appreciable changes in the lattice parameters or cell volume for cobalt and nickel doped (up to 9 mol %) compounds. In Table 2, we have summarized the Rietveld refined structural parameters for the representative $Zn_{0.95}Co_{0.05}O$ compound. Observed, calculated, and the different XRD patterns for (a) Undoped ZnO, (b) $Zn_{0.95}Co_{0.05}O$, and (c) $Zn_{0.95}Ni_{0.05}O$ compounds are shown in Figure 2. There was a good agreement between the observed and calculated patterns except small impurity of NiO around 2 theta 37 and 43 (Figure 2 (c)). The wurtzite hexagonal crystal structure of $Zn_{0.95}Co_{0.05}O$ compound was modeled by using Visualization for electronic structural analysis (VESTA) program (Figure 2(d)). In the wurtzite hexagonal structure of ZnO, Zn^{2+}/Co^{3+} atoms were bonded to four O^{2-} atoms in tetrahedral configuration. On doping with cobalt and nickel ions to zinc site in the ZnO system, we did not observe any structural transition or modification of wurtzite hexagonal structure. The average crystallite size was calculated using the Scheerrer equation,

$$D = k\lambda/\beta Cos\theta \quad (3)$$

Where D is the crystallite size, k is the Scherrer constant (0.9), λ is the X-ray wavelength, θ is the Bragg angle and β is the corrected full-width half-maxima of the sample. The average crystallite sizes were to 17 to 33 nm. The values are presented in Table 3. Observed, calculated and the difference XRD

Table 1. Rietveld refined lattice parameters and unit cell volume for undoped, Co and Ni doped ZnO NPs.

Compounds	Lattice Parameters (Å)*a* *c*		Unit cell volume (Å^3)
ZnO (un-doped)	3.250(4)	5.206(1)	47.62(4)
$Zn_{0.99}Co_{0.01}O$	3.250(1)	5.206(4)	47.62(5)
$Zn_{0.97}Co_{0.03}O$	3.250(2)	5.206(6)	47.62(4)
$Zn_{0.95}Co_{0.05}O$	3.250(2)	5.206(5)	47.62(2)
$Zn_{0.93}Co_{0.07}O$	3.251(5)	5.207(6)	47.66(2)
$Zn_{0.91}Co_{0.09}O$	3.252(8)	5.208(2)	47.70(6)
$Zn_{0.99}Ni_{0.01}O$	3.250(2)	5.202(5)	47.59(6)
$Zn_{0.97}Ni_{0.03}O$	3.250(3)	5.203(6)	47.60(3)
$Zn_{0.95}Ni_{0.05}O$	3.251(5)	5.203(4)	47.62(8)
$Zn_{0.93}Ni_{0.07}O$	3.252(5)	5.204(6)	47.64(2)
$Zn_{0.91}Ni_{0.09}O$	3.249(7)	5.201(4)	47.56(4)

Table 2. Rietveld refined structural parameters for 5 mol % cobalt – doped ZnO NPs ($Zn_{0.95}Co_{0.05}O$).

Atoms	Oxidation State	Wyckoff notations	x	y	z	B_{iso}	Occupancy
Zn	2	(2b)	0.3333	0.6667	0.0000	0.500	0.95
Co	3	(2b)	0.3333	0.6667	0.0000	0.500	0.05
O	−2	(2b)	0.3333	0.6667	0.3812(7)	0.500	1.00

Crystal system = Hexagonal, Space group = *P63 mc* (No. 186);
Lattice parameters: a = 3.251(3) Å, c = 5.206(8) Å; Cell volume = 47.66(2) Å^3
R factors (%): R_p = 4.53, R_{wp} = 6.14, $R_{Exp.}$ = 5.67, χ2 = 1.18, R_{Bragg} = 3.50, R_F = 6.77

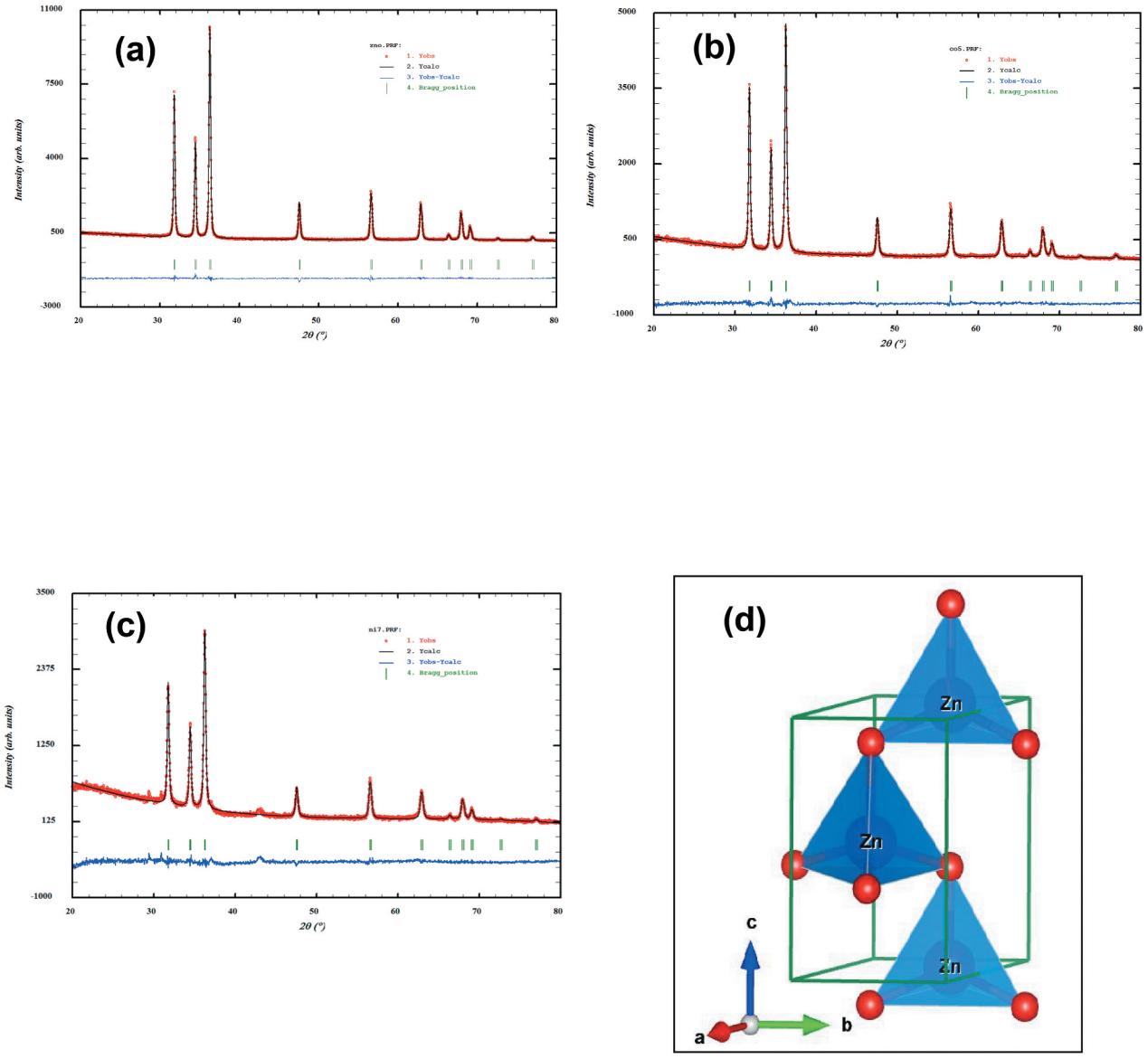

Figure 2. Observed, calculated and the difference X-ray diffraction patterns of (a) ZnO, (b) $Zn_{0.95}Co_{0.05}O$, (c) $Zn_{0.95}Ni_{0.05}O$ and (d) Crystal structure of $Zn_{0.95}Co_{0.05}O$ NPs.

Table 3. Average crystallite size of undoped, Co and Ni doped ZnO NPs.

Sample	Average crystallite size (nm)
ZnO (un-doped)	33.2
$Zn_{0.99}Co_{0.01}O$	28.8
$Zn_{0.97}Co_{0.03}O$	28.1
$Zn_{0.95}Co_{0.05}O$	27.7
$Zn_{0.93}Co_{0.07}O$	27.0
$Zn_{0.91}Co_{0.09}O$	24.4
$Zn_{0.99}Ni_{0.01}O$	29.7
$Zn_{0.97}Ni_{0.03}O$	25.5
$Zn_{0.95}Ni_{0.05}O$	24.6
$Zn_{0.93}Ni_{0.07}O$	22.6
$Zn_{0.91}Ni_{0.09}O$	17.1

patterns for all the Co and Ni doped ZnO NPs are provided in supplementary file.

3.2. Morphology

The FE-SEM micrographs of undoped ZnO NPs, and Co and Ni-doped ZnO NPs are shown in Figure 3a(a-k). These micrographs showed the crystalline powder which was shaped spherically. Aside from this, the powder contained several voids or holes together, the reason that can be due to the discharge of hot gases that escape during the combustion from the reaction mixture. It absolutely was through these pores of varied size and form the crystallites were interlinked to one another. SEM micrographs delineated that the particles were collective with spongy cave-like structures. It conjointly indicated that sinterable tendency had hyperbolic

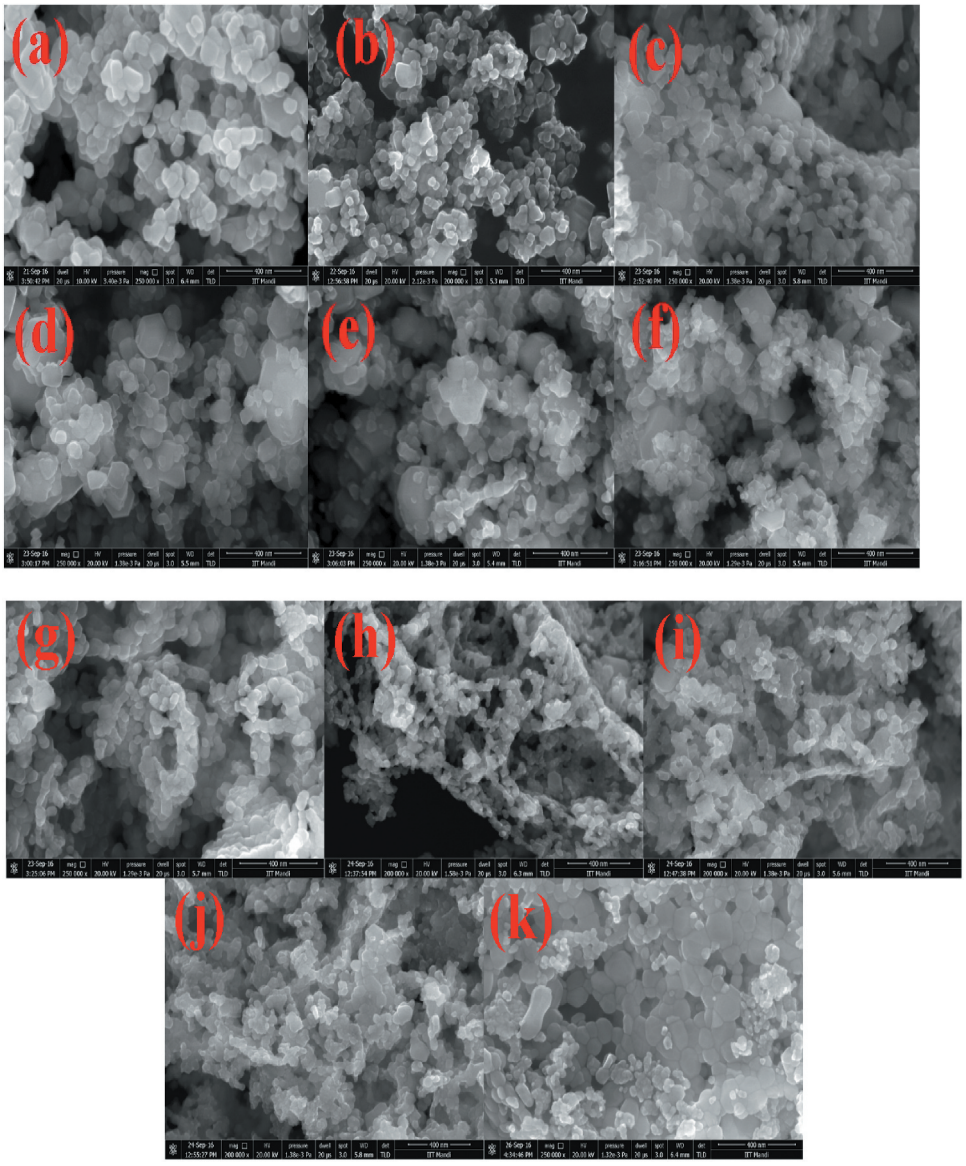

Figure 3. FESEM images of (a) ZnO undoped, (b) $Zn_{0.99}Co_{0.01}O$, (c) $Zn_{0.97}Co_{0.03}O$, (d) $Zn_{0.95}Co_{0.05}O$, (e) $Zn_{0.93}Co_{0.07}O$, (f) $Zn_{0.91}Co_{0.09}O$, (g) $Zn_{0.99}Ni_{0.01}O$, (h) $Zn_{0.97}Ni_{0.03}O$, (i) $Zn_{0.95}Ni_{0.05}O$, (j) $Zn_{0.93}Ni_{0.07}O$ and (k) $Zn_{0.91}Ni_{0.09}O$, EDS of (l) ZnO undoped, (m) $Zn_{0.99}Co_{0.01}O$, (n) $Zn_{0.97}Co_{0.03}O$, (o) $Zn_{0.95}Co_{0.05}O$, (p) $Zn_{0.93}Co_{0.07}O$, (q) $Zn_{0.91}Co_{0.09}O$, (r) $Zn_{0.99}Ni_{0.01}O$, (s) $Zn_{0.97}Ni_{0.03}O$, (t) $Zn_{0.95}Ni_{0.05}O$, (u) $Zn_{0.93}Ni_{0.07}O$ and (v) $Zn_{0.91}Ni_{0.09}O$.

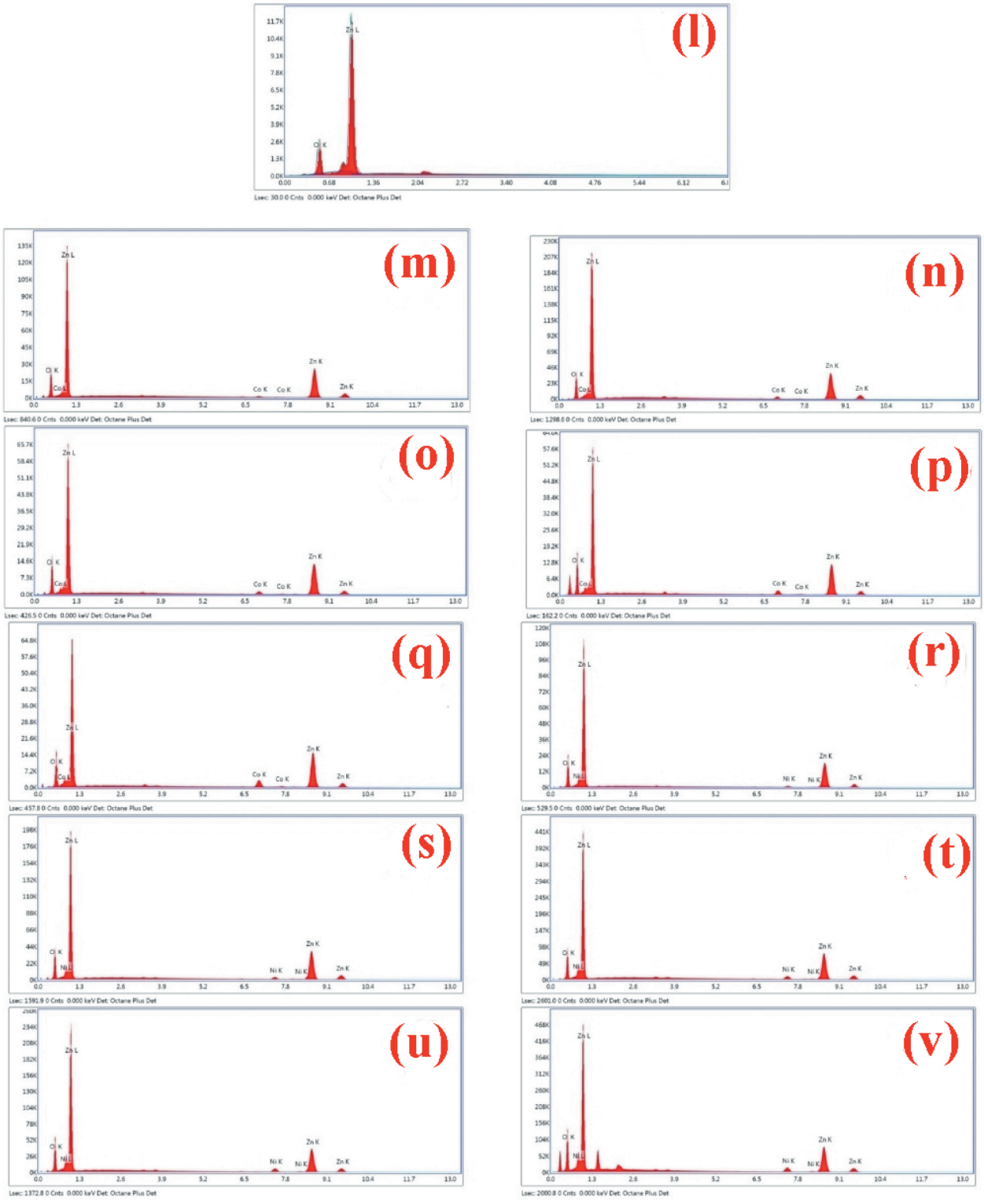

Figure 3b. (continued).

to make the part forge agglomerates. This tendency could be because of increase in surface energy that was the thrust for sintering in combustion method [39]. EDS data of the NPs is given in Figure 3b(l-v) and Table 4. The EDS spectra showed signals of all the expected elements Zn, O, Co and Ni and confirmed the presence of Co^{2+} and Ni^{2+} ions that were substituting the Zn^{2+} ions in the Zn matrix. Hence, the results concluded that Co and Ni ions have been doped into the ZnO lattice without any impurities. Elemental mapping is shown in Figure 4(a-k). They proved the homogenous distribution of elements Zn, O, Co, and Ni in the prepared samples. ICP-OES data given in Table 5 quantified the elemental concentrations of Co and Ni in all the doped samples.

Table 4. EDS data of undoped, Co and Ni doped ZnO NPs.

Sample	Element	Weight %
ZnO (un-doped)	O	22.16
	Zn	77.84
$Zn_{0.99}Co_{0.01}O$	O	26.55
	Co	1.33
	Zn	72.11
$Zn_{0.97}Co_{0.03}O$	O	16.49
	Co	1.76
	Zn	81.75
$Zn_{0.95}Co_{0.05}O$	O	25.32
	Co	4.71
	Zn	69.97
$Zn_{0.93}Co_{0.07}O$	O	20.15
	Co	3.67
	Zn	76.19
$Zn_{0.91}Co_{0.09}O$	O	17.39
	Co	5.52
	Zn	77.09
$Zn_{0.99}Ni_{0.01}O$	O	30.20
	Ni	3.31
	Zn	66.49
$Zn_{0.97}Ni_{0.03}O$	O	16.43
	Ni	3.29
	Zn	80.27
$Zn_{0.95}Ni_{0.05}O$	O	18.32
	Ni	2.73
	Zn	78.95
$Zn_{0.93}Ni_{0.07}O$	O	21.95
	Ni	3.33
	Zn	74.72
$Zn_{0.91}Ni_{0.09}O$	O	23.83
	Ni	4.02
	Zn	72.15

3.3. Effect of doping and UV exposure on the anti-bacterial activity

Results of undoped and doped antibacterial activity of the ZnO NPs shown in Figure 5 Suggest that both Co and Ni doping increased the antibacterial ability of ZnO NPs against both bacterial species, e.g., *S. enterica* and *C. perfringens* as indicated by ≥ 2-fold reduction in MIC values. UV exposure further increased the antibacterial activity as indicated by additional 2-fold reduction (a total 4 fold reduction) in MICs as compared to undoped ZnO NPs. Highest increase in the anti-bacterial activity was noticed with doping with Co 1 mol % after UV exposure, as shown by 8-fold decline in the MIC (15.62 µg/mL) as compared to un-doped/un-exposed ZnO NPs (125.0 µg/mL)

Together results suggest that doping is beneficial from the view point of antibacterial activity of ZnO NPs. UV exposure further added to this increase in anti-bacterial activity.

The precise mechanism of ZnO's bioactivity is still being debated. Many processes related to this have been suggested. The two key possible mechanisms of the interaction between NPs and bacteria suggested by several investigations are (i) the production of increased levels of ROS, mostly hydroxyl radicals, and singlet oxygen [40–43] and (ii) cell membrane zinc toxicity by adhesion of ZnO particles inhibiting bacterial growth [44,45].

3.4. Effect of doping and UV exposure on the cytotoxicity of ZnO NPs toward normal and cancer cells

Effect of UV exposure on the cytotoxicity potential (measured as IC50 values) of undoped or doped ZnO NPs toward normal and cancer cells are shown in Figure 6. Effects of doping and UV exposure on the ZnO NPs for their cytotoxicity toward Normal 3T3-L1 as well as cancer (HeLa and MCF-7) cells were compared considering the IC50 concentration of undoped and non-UV exposed ZnO NPs, e.g., 320 µg/mL as 100%.

In normal cell *(3T3-L1)*: Toward normal 3T3-L1 cells, higher declines in IC50 of ZnO NPs were observed with higher doping concentrations, i.e., 9 mol %, of Ni (50%) and Co (37.5%). UV exposure showed only limited effect on the IC50 of ZnO NPs, difference in decline between Un-exposed and UV-exposed, in IC50 concentrations was 25% in case of undoped NPs and 12.5 to 25% in case of Co-doped, whereas no effect was observed with Ni-doped NPs. Results suggest that doping increased cytotoxicity of ZnO NPs toward normal cells. However, not much impact of UV exposure was observed as evident by minor lowerings (0 to 25%) in IC50 concentrations.

In cancer cells: In case of cancer cells, doping with higher concentrations (9 mol %) of both Co and Ni, caused 75% decline in IC50 concentration toward HeLa

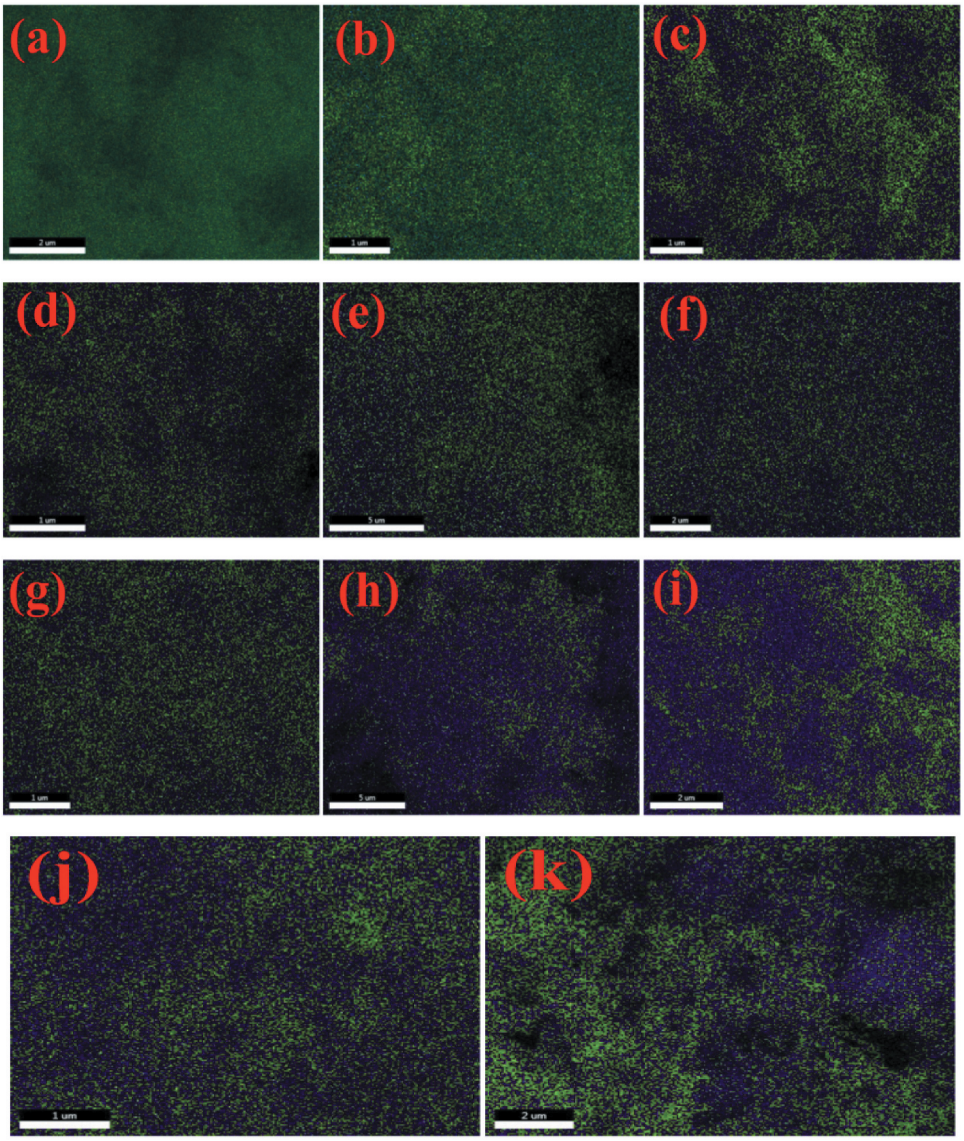

Figure 4. Elemental mapping of (a) ZnO undoped, (b) $Zn_{0.99}Co_{0.01}O$, (c) $Zn_{0.97}Co_{0.03}O$, (d) $Zn_{0.95}Co_{0.05}O$, (e) $Zn_{0.93}Co_{0.07}O$, (f) $Zn_{0.91}Co_{0.09}O$, (g) $Zn_{0.99}Ni_{0.01}O$, (h) $Zn_{0.97}Ni_{0.03}O$, (i) $Zn_{0.95}Ni_{0.05}O$, (j) $Zn_{0.93}Ni_{0.07}O$ and (k) $Zn_{0.91}Ni_{0.09}O$.

Table 5. ICP-OES data of undoped, Co and Ni doped ZnO NPs (calculated and observed values).

		Weight %	
Sample	Element	Calculated	Observed (Instrumental value)
ZnO (un-doped)	Zn	80.33	79.99
$Zn_{0.99}Co_{0.01}O$	Co	0.72	0.7819
	Zn	79.62	79.75
$Zn_{0.97}Co_{0.03}O$	Co	2.17	2.34
	Zn	78.11	77.8
$Zn_{0.95}Co_{0.05}O$	Co	3.63	3.87
	Zn	73.62	74.75
$Zn_{0.93}Co_{0.07}O$	Co	5.09	5.91
	Zn	75.13	74.52
$Zn_{0.91}Co_{0.09}O$	Co	6.56	6.608
	Zn	73.63	72.42
$Zn_{0.99}Ni_{0.01}O$	Ni	0.72	1.13
	Zn	79.6	78.91
$Zn_{0.97}Ni_{0.03}O$	Ni	2.16	2.44
	Zn	78.12	78.92
$Zn_{0.95}Ni_{0.05}O$	Ni	3.62	4.14
	Zn	76.63	77.18
$Zn_{0.93}Ni_{0.07}O$	Ni	5.077	5.15
	Zn	75.14	74.88
$Zn_{0.91}Ni_{0.09}O$	Ni	6.539	6.08
	Zn	73.65	72.98

Element symbol wavelength of Zn: 206.2 nm, Co: 228.616 nm and Ni: 231.604 nm

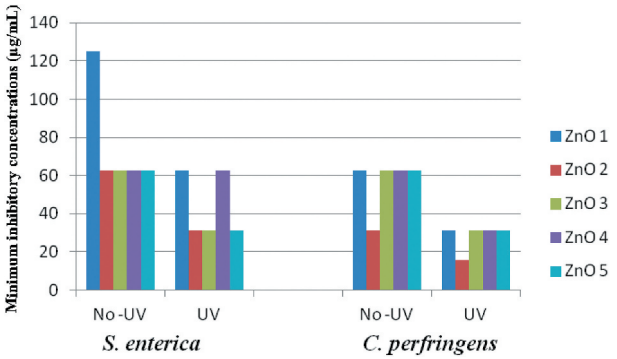

Figure 5. Effect of doping (with Co or Ni) and UV exposure on the Inhibitory potential (MICs) of ZnO NPs on the bacteria, *S. enterica* and C. *perfringens.*

cells and 68.75% (Co) and 62.50% (Ni) toward MCF-7 cells. UV exposure further lowered down IC50 concentrations of NPs doped with lower concentrations (1 mol %) of Co and Ni. Effect of UV exposure was more prominent with MCF-7 cells, where doping with Ni at both concentrations (1 and 9 mol %) has not shown any effect on IC50 concentrations. Results suggest a higher impact of doping as well as UV exposure in lowering IC50 concentrations of ZnO NPs toward cancer cells. Impact of UV exposure was more obvious with MCF-7 cells.

Together, results, suggest that, the exposure of UV radiations lowered the IC50 of undoped ZnO NPs toward normal cells only by 25%, whereas reduced IC50 concentrations by 50% and 68.75%, respectively, toward HeLa and MCF-7 cells. Among the doped NPs, those doped with 1 mol % of Ni showed minimum reduction in IC50 toward Normal cells (25%) compared to higher reductions in case of cancer cells, e.g., 50% for Hela cells and 62.5% for MCF-7 cells. Finally, it can be concluded, that, UV exposure played important role in enhancing cytotoxicity as evident by significant lowering in IC50 concentrations of both undoped or doped ZnO NPs toward cancer cells, whereas doping did not appear to enhance cytotoxicity of ZnO NPs.

Literature shows that ZnO NPs induce toxicity in associate extremely cell-specific and proliferation dependent manner by rapidly dividing cancer cells being the foremost prone and quiescent cells being the least sensitive [46,47]. Rasmussen et al. (2016) have summarized the mechanisms of various medical applications of ZnO nanomaterials particularly against neoplasm, and cancer together with brain tumor, breast, bone, colon, and cancer and lymphomas [48]. The surface chemistry of ZnO NPs might have made them targeting specific proteins or chemical groups in tumor cells instead of normal ones. This high degree of selective killing of cancer cell found to be dependent on the proliferation status of cells, with rapidly dividing cells being the most susceptible [48].

[Difference in IC50 value due to UV exposure or doping and results of the effect of UV exposure tested at different time intervals by carrying out the MTT assay are provided in supplementary file].

3.5. Effect of doping and UV exposure on the ROS generation by J774 mouse macrophage cells

Results of ROS generation are depicted in Figure 7. Data showed the effect of exposure of UV radiations on the capacity of ZnO NPs, both undoped as well as doped ones, on the ROS generation by the murine macrophage cells. Data suggested that UV-exposed undoped ZnO NPs induced increased ROS generation as compared to UV-unexposed samples at 50.0 µg/mL followed by a drastic fall at lower concentrations, e.g., 25.0 and 12.5 µg/mL.

NPs doped with 9 and 1 mol % Co showed higher RFUs as compared to undoped NPs at all the tested

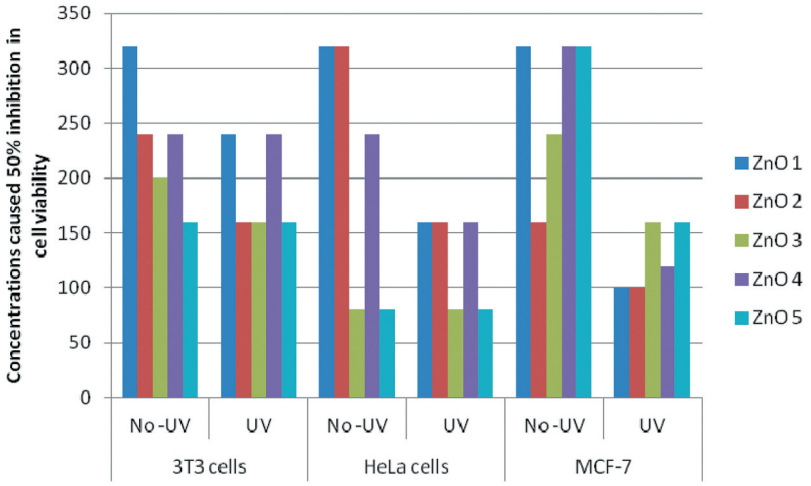

Figure 6. Effect of doping (with Co or Ni) and UV exposure on the cytotoxicity of ZnO NPs on normal (3T3 L1) and cancer (HeLa and MCF-7) cells.

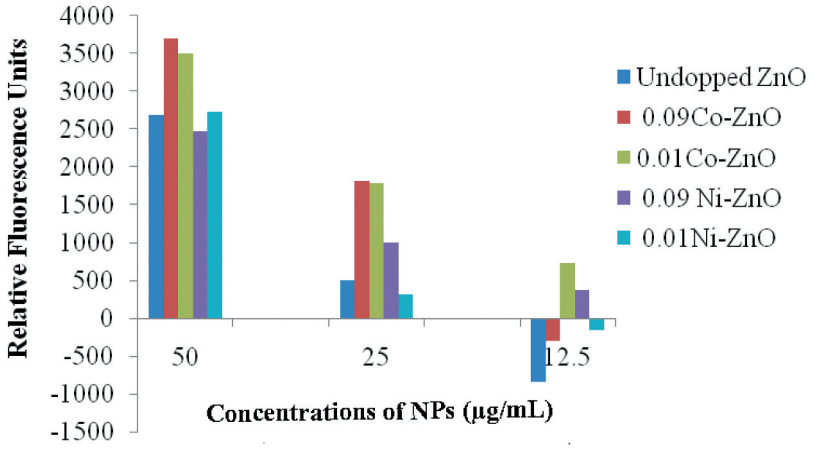

Figure 7. Effect of doping (with Cobalt or Nickel) and UV exposure on the Reactive Oxygen Species (ROS) generation inducing activity of ZnO NPs in J774 mouse macrophage cells.

concentrations. Among the two doping concentrations, 9 mol % showed only marginally higher ROS generation at 50.0 and 25.0 µg/mL concentrations. However, at 12.5 µg/mL doping with 1 mol % Co was found greater than that doped with 9 mol % Co suggesting better doping with lesser concentration of Cobalt, i.e. 1 mol %.

Similarly, doping with Ni also increased the potential of ZnO NPs toward inducing ROS generation by macrophage cells as compared to undoped NPs. At 50.0 µg/mL concentration doping with lesser Ni, i.e., 1 mol % showed higher difference (2723) than its higher doping, i.e., 9 mol %. However, at lower test concentrations, e.g., 25.0 and 12.5 µg/mL, doping with higher Ni, i.e., 9 mol % showed higher induction in ROS generation.

Together results revealed that, doped ZnO NPs enhanced the oxidative response of mouse macrophage cells by increasing the ROS generation. Importantly, doping of NPs caused a slow and steady fall in ROS generation unlike undoped ones which showed sudden fall, on sequential (2 fold) decrease in the test concentrations. Also, doping with cobalt was found better than the nickel in inducing such effect.

4. Conclusions

The present research was conducted to assess the anti-bacterial, anti-cancer, and oxidative response generation activities of undoped, Co- or Ni-doped ZnO NPs prepared by the combustion synthesis using a bio fuel as reductant. We wanted to understand the underlying mechanism behind enhanced activity. We understood that UV radiations active materials can have elevated oxygen vacancies which can induce ROS generation in biological systems and therefore, tested the Un-doped/doped ZnO NPs for the same activities after UV exposure. Experimental results indicated that the incorporation of Co and Ni into the ZnO NPs matrix increased their antibacterial activity against *S. enterica* and *C. perfringens* and cytotoxic effect on HeLa and MCF-7 cells as compared to undoped ZnO NPs. Further, it was also observed that, UV-exposed ZnO NPs had the highest antibacterial and anticancer activity as compared to UV-unexposed ones. Further, results also revealed that, doped ZnO NPs induced the enhanced oxidative response in mouse macrophage cells as evidenced by the increased ROS generation. Importantly, doping of NPs caused a slow and steady fall in ROS generation unlike undoped ones which showed sudden fall, on sequential (2 fold) decrease in the test concentrations. Further experiments will resolve the understanding regarding how these particles can behave in biological (*in-vivo*) system. However, data of this study indicate that on one side ZnO NPs showed direct activity against bacteria and cancer cells, whereas on the other hand, capable of boosting host's immunity via inducing activation of immune cells as evident by increased ROS generation by mouse macrophage cells.

Acknowledgments

The authors thank Dr. Tejabhiram Yadavalli, Department of Ophthalmology and Visual Sciences, University of Illinois, Chicago, USA for his valuable suggestions. The author Dr. G.K. Prashanth thanks management of Sri KET, Bengaluru for the support and encouragement extended towards this project. The authors acknowledge TIFR, Mumbai for PXRD, IIT Mandi for, FESEM and elemental mapping, IIT Madras for ICP-OES measurements. Dr. Padam Singh was an SRF, UGC, New Delhi, India.

Author contributions

Dr. G.K. Prashanth, Dr. Vinita Chaturvedi and Dr. P.A. Prashanth conceptualized the study. Dr. G.K. Prashanth, Dr. Vinita Chaturvedi, Dr. P.A. Prashanth and Dr. C. Shivakumara wrote

the manuscript. All the authors conducted the experiments and all have reviewed the manuscript.

Ethics approval

Not required.

Disclosure statement

The authors declare that they have no known competing financial interests or personal relationships that could have appeared to influence the work reported in this paper.

References

[1] Yadavalli T, Shukla D. Role of metal and metal oxide nanoparticles as diagnostic and therapeutic tools for highly prevalent viral infections. Nanomed Nanotechnol Biol Med. 2017;13(1):219–230.

[2] Yadavalli T, Shukla D. Could zinc oxide tetrapod nanoparticles be used as an effective immunotherapy against HSV-2? Nanomedicine. 2006;11:2239–2242.

[3] Duggal N, Jaishankar D, Yadavalli T, et al. Zinc oxide tetrapods inhibit herpes simplex virus infection of cultured corneas. Mol Vis. 2017;23:26–38.

[4] Antoine TE, Hadigal SR, Abraam Yakoub YK, et al. Intravaginal zinc oxide tetrapod nanoparticles as novel immunoprotective agents against Genital Herpes. J Immunol. 2016;196(11):4566–4575.

[5] Oves M, Mohd Arshad MS, Khan AS, et al. Ismail, Antimicrobial activity of cobalt doped zinc oxide nanoparticles: targeting water borne bacteria. J Saudi Chem Soc. 2015;19(5):581–588.

[6] Dinesha ML, Jayanna HS, Mohanty S, et al. Structural, electrical and magnetic properties of Co and Fe codoped ZnO nanoparticles prepared by solution combustion method. J Alloys Compounds. 2010;490(1–2):618–623.

[7] Mohamed Basith N, Judith Vijaya J, John Kennedy L, et al. Co-Doped ZnO Nanoparticles: structural,morphological,optical,magneticand antibacterial studies. J Mater Sci Technol. 2014;30:1108–1117.

[8] Shruti, Vimala R. Synthesis of nickel doped ZnO nanoparticles by hydrothermal decomposition of zinc hydroxide nitrate and its antimicrobial assay. Int J Pure App Biosci. 2015;3:186–190.

[9] Saravana Kumar R, Dananjaya SHS, De Zoysa M, et al. Enhanced antifungal activity of Ni-doped ZnO nanostructures under dark conditions. RSC Adv. 2016;10:108468–108476.

[10] Nehru LC, Sanjeeviraja C. ZnO nanoparticles by citric acid assisted microwave solution combustion method. J Ceramic Process Res. 2013;6:712–716.

[11] Özdemir H, Faruk Öksüzömer MA. Synthesis of Al_2O_3, MgO and $MgAl_2O_4$ by solution combustion method and investigation of performances in partial oxidation of methane. Powder Technol. 2020;359:107–117.

[12] Patil KC, Aruna SC, Mimani T. Combustion synthesis: an update. Curr Opin Solid State Mater Sci. 2002;6(6):507–512.

[13] Patil KC, Hegde MS, Tanu R, et al. Chemistry of nanocrystalline oxide materials. Singapore: World Scientific; 2008.

[14] Prashanth GK, Prashanth PA, Nagabhushana BM, et al. Comparison of anticancer activity of biocompatible ZnO nanoparticles prepared by solution combustion synthesis using aqueous leaf extracts of *Abutilon indicum, Melia azedarach* and *Indigofera tinctoria* as bio-fuels, Artificial Cells. Nanomed Biotechnol. 2018;46:968–979.

[15] Mukherjee S, Sushma V, Patra S, et al. Green chemistry approach for the synthesis and stabilization of biocompatible gold nanoparticles and their potential applications in cancer therapy. Nanotechnology. 2012;23(45):455103.

[16] Sudip Mukherjee B, Vinothkumar SP, Bangal PR, et al. Potential therapeutic and diagnostic applications of one-step in situ biosynthesized gold nanoconjugates (2-in-1 system) in cancer treatment. RSC Adv. 2013;3:2318–2329.

[17] Mukherjee S, Chowdhury D, Kotcherlakota R, et al. Potential theranostics application of biosynthesized silver nanoparticles (4-in-1system). Theranostics. 2014;4(3):316–335.

[18] Lee J, Kim HY, Zhou H, et al. Jaebeom Lee Green synthesis of phytochemicalstabilized Au nanoparticles under ambient conditions and their biocompatibility and antioxidative activity. J Mater Chem. 2011;21(35):13316–13326.

[19] Shankar SS, Ahmad A, Pasricha R, et al. Bioreduction of chloroaurate ions by geranium leaves and its endophytic fungus yields gold nanoparticles of different shapes. J Mater Chem. 2003;13(7):1822–1826.

[20] Ahmad A, Senapati S, Khan MI, et al. Extra-/intracellular biosynthesis of gold nanoparticles by an Alkalotolerant Fungus, *Trichothecium* sp. J Biomed Nanotechnol. 2006;1(1):47–53.

[21] Patra S, Mukherjee S, Barui AK, et al. Green synthesis, characterizationof gold and silver nanoparticles and their potential application for cancer therapeutics. Mater Sci Eng C. 2015;53:298–309.

[22] Noruzi M, Zare D, Khoshnevisan K, et al. Rapid green synthesis of gold nanoparticles using Rosa hybrida petal extract at room temperature. Spectrochim Acta A Mol Biomol Spectrosc. 2011;79(5):1461–1465.

[23] Montes MO, Mayoral A, Deepak FL, et al. Anisotropic gold nanoparticles and gold plates biosynthesis using alfalfa extracts. J Nanopart Res. 2011;13(8):3113–3121.

[24] Prashanth GK, Prashanth PA, Bora U, et al. In vitro antibacterial and cytotoxicity studies of ZnO nanopowders prepared by combustion assisted facile green synthesis. Karbala Int J Modern Sci. 2015;1(2):67–77.

[25] Saravanakumar A, Peng MM, Ganesh M, et al. Low-cost and eco friendly green synthesis of silver nanoparticles using *Prunus japonica* (Rosaceae) leaf extract and their antibacterial, antioxidant properties. Artif Cells Nanomed Biotechnol. 2016;45:1165–1171.

[26] Sathishkumar G, Logeshwaran V, Sarathbabu S, et al. Green synthesis of magnetic Fe_3O_4 nanoparticles using *Couroupita guianensis Aubl*. fruit extract for their antibacterial and cytotoxicity activities. Artif Cells Nanomed Biotechnol. 2017;46(3):589–598.

[27] Singh H, Du J, Yi TH. Green and rapid synthesis of silver nanoparticles using Borago officinalis leaf extract: anticancer and antibacterial activities. Artif Cells Nanomed Biotechnol. 2016;45(7):1310–1316.

[28] Krishna PG, Ananthaswamy PP, Trivedi P, et al. Amani Erra and Tejabhiram Yadavalll, Anti-tubercular activity of ZnO nanoparticles prepared by solution combustion synthesis using lemon juice as bio-fuel. Mater Sci Eng C. 2017;75:1026–1033.

[29] Al Banna LS, Salem NM, Jaleel GA, et al. Green synthesis of sulfur nanoparticles using Rosmarinus officinalis leaves extract and nematicidal activity against *Meloidogyne javanica*. Chem Int. 2020;6:137.
[30] Awwad AM, Amer MW, Salem NM, et al. Green synthesis of zinc oxide nanoparticles (ZnO-NPs) using *Ailanthus altissima* fruit extracts and antibacterial activity. Chem Int. 2020;6:151–159.
[31] Singh P. Green synthesis and characterization of silver nanoparticles by using aloe vera plant extract. Trends in Drug Deliver. 2019;6:30–35.
[32] Özdemir AAS, Gülcan M, Cellat K, et al. Synthesis and characterization of Reishi mushroom-mediated green synthesis of silver nanoparticles for the biochemical applications. J Pharm Biomed Anal. 2020;178:112970.
[33] Prashanth GK, Prashanth PA, Meghana Ramani S, et al. Comparison of antimicrobial, antioxidant and anticancer activities of ZnO nanoparticles prepared by lemon juice and citric acid fueled solution combustion synthesis. BioNanoSci. 2019;9:799–812.
[34] Krishna PG, Ananthaswamy PP, Yadavalli T, et al. ZnO nanopellets have selective anticancer activity. Mater Sci Eng C. 2016;62:919–926.
[35] Krishna PG, Ananthaswamy PP, Gadewar M, et al. In vitro antibacterial and anticancer studies of ZnO nanoparticles prepared by sugar fueled combustion synthesis. Adv Mater Lett. 2017;8(1):24–29.
[36] Prashanth GK, Prashanth PA, Nagabhushana BM, et al. In vitro antimicrobial, antioxidant and anticancer studies of ZnO nanoparticles synthesized by precipitation method. Adv Sci Eng Med. 2016;8:306–313.
[37] Krishna PG, Ananthaswamy PP, Mutta NB, et al. Comparison of antimicrobial and anticancer activity of ZnO nanoparticles prepared using different precursors by hydrothermal synthesis. JCHPS. 2017;10:192–197.
[38] Basu SK, Kumar D, Singh DK, et al. Mycobacterium tuberculosis secreted antigen (MTSA-10) modulates macrophage function by redox regulation of phosphatases. Febs J. 2006;273(24):5517–5534.
[39] Roy TK, Bhowmick D, Sanyal D, et al. Sintering studies of nano-crystalline zinc oxide. Ceramics Int. 2008;34(1):81–87.
[40] Heinlaan M, Ivask A, Blinova I, et al. Toxicity of nanosized and bulk ZnO, CuO and TiO_2 to bacteria *Vibrio fischeri* and crustaceans Daphnia magna and Thamnocephalus platyurus. Chemosphere. 2008;71(7):1308–1316.
[41] Yang H, Liu C, Yang D, et al. Comparative study of cytotoxicity, oxidative stress and genotoxicity induced by four typical nanomaterials: the role of particle size, shape and composition. J Appl Toxicol. 2009;29(1):69–78.
[42] Akhavan O, Mehrabian M, Mirabbaszadeh K, et al. Hydrothermal synthesis of ZnO nanorod arrays for photocatalytic inactivation of bacteria. J Phys D: App Phys. 2009;42(22):225305.
[43] Franklin NM, Rogers NJ, Apte SC, et al. Comparative toxicity of nanoparticulate ZnO, Bulk ZnO, and ZnCl2 to a Freshwater Microalga (Pseudokirchneriella subcapitata): the importance of particle solubility. Sci Technol. 2007;41(24):8484–8490.
[44] Xu T, Xie CS. Tetrapod-like nano-particle ZnO/acrylic resin composite and its multi-function property. Prog Org Coat. 2003;46(4):297–301.
[45] Zhang LL, Jiang YH, Ding YL, et al. Investigations into the antibacterial behavior of suspensions of ZnO nanoparticles (ZnO nanofluids). J Nanoparticles. 2007;9(3):479–489.
[46] Premanathan M, Karthikeyan K, Jeyasubramanian K, et al. Selective toxicity of ZnO nanoparticles toward Gram positive bacteria and cancer cells by apoptosis through lipid peroxidation. Nanomedicine. 2011;7(2):184–192.
[47] Hanley C, Layne J, Alex Punnoose KM, et al. Preferential killing of cancer cells and activated human T cells using ZnO nanoparticles. Nanotechnol. 2008;19(29):295103.
[48] Rasmussen K, Gonzalez M, Kearns P, et al. Review of achievements of the OECD working party on manufactured nanomaterials' testing and assessment programme. From exploratory testing to test guidelines. Regul Toxicol Pharmacol. 2016;74:147–160.